Yamamoto *et al. Earth, Planets and Space* (2021) 73:169
https://doi.org/10.1186/s40623-021-01505-1

Earth, Planets and Space

EXPRESS LETTER

Open Access

Temporal variations of magma composition, eruption style and rate at Fuji Volcano, Japan

Takahiro Yamamoto*, Shun Nakano and Yoshihiro Ishizuka

Abstract

Mt. Fuji is an active basaltic volcano near the Tokyo metropolitan area; future eruptions could thus have serious nationwide impacts. To better understand recent volcanism at Fuji Volcano, we here clarify temporal variations of eruption rate and magma composition since 5.6 ka based on time-series volumetric and geochemical data of eruptive products in a new stratigraphic sequence. Volcanic activity during the studied period consisted of (i) the emission of many lava flows that formed a new volcanic edifice between 5.6 and 3.45 ka, (ii) a period dominated by explosive events both at the summit and on the flanks of the volcano between 3.45 and 2.25 ka, and (iii) a period dominated by flank fissure eruptions since 2.25 ka. The eruption rate (dense-rock equivalent, DRE) was 3.5 km^3 DRE/kyr during the edifice-building period, decreased to 0.8 km^3 DRE/kyr during the explosive period, and then increased to 2.0 km^3 DRE/kyr since 1.5 ka. Erupted magmas were dominantly basaltic and geochemically similar through time, except for increased Sr contents and decreased Ca/Sr ratios during the explosive period. Similarly, the geochemical properties of the parental magmas did not change greatly, although the Sr contents and Ca/Sr ratios of magmas erupted during the explosive period reflect the delayed fractionation of plagioclase due to the increased water contents of the parental magmas at that time.

Keywords: Fuji Volcano, Eruptive history, Eruption rate, Magma composition, Japan

Main text

Introduction

Mt. Fuji is the largest active stratovolcano in Japan and has been dormant since the AD 1707 Hoei eruption (Miyaji 2011). Although there are no superficial signs of volcanic activity, deep low-frequency seismicity occurred frequently beneath Fuji Volcano between 2000 and 2001 (Ukawa 2005). An eruption of similar scale to the Hoei one, would cause great impacts nowadays, especially because of volcanic ashfall that could occur within the entire nation and especially within the nearby Tokyo metropolitan area, which is situated 100 km to the east of the volcano (Yamamoto and Nakada 2015). In response to the 2000–2001 seismicity, the Japanese Government founded the Review Committee of Volcanic Hazard Mitigation of Fuji Volcano and, in 2004, published the first edition of the hazard map based on available findings at that time. Subsequently, the Geological Survey of Japan performed field surveys and trench excavations of the entire volcanic area and revised the geological map of Fuji Volcano with new stratigraphic division of the Hoshiyama, Fujinomiya and Subashiri stages (Fig. 1; Takada et al. 2016). Based on this eruptive history, the hazard map was updated in March 2021 by the Shizuoka and Yamanashi Prefectures.

Fuji Volcano is situated in the zone of the collision between the Northeast Japan and Izu-Mariana arcs (Fig. 1). Magmatic activity at Fuji results from the subduction of the Pacific slab beneath the Eurasian and Philippine Sea plates (Fujii 2007). Erupted magmas are petrologically characterized by highly differentiated basaltic magmas with FeO*/MgO ratios > 1.5 and containing abundant incompatible elements (Togashi and Takahashi 2007; Fujii 2007). Here, based on volumetric

*Correspondence: t-yamamoto@aist.go.jp
Geological Survey of Japan, AIST, Higashi 1-1-1 Central 7, Tsukuba 305-5867, Japan

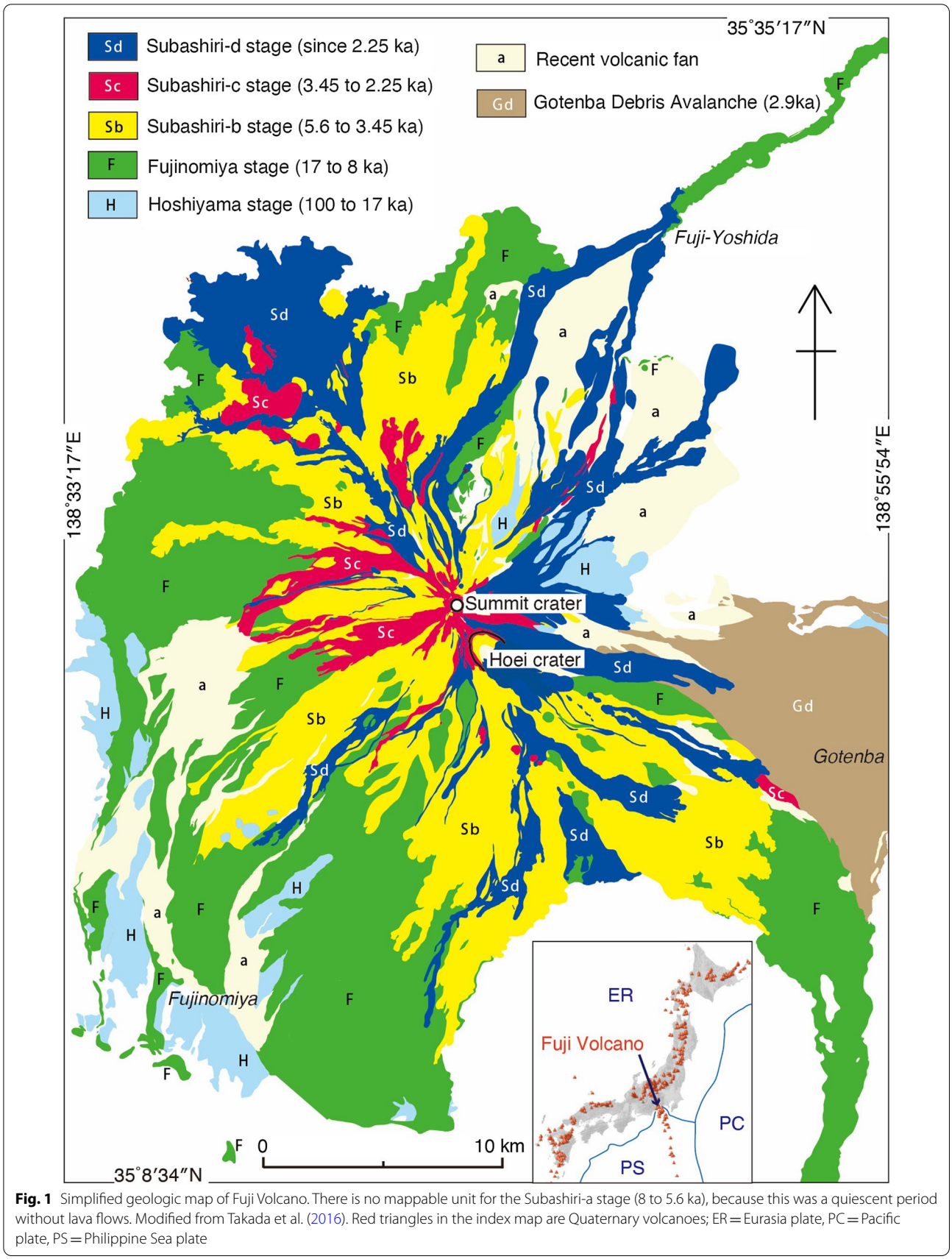

Fig. 1 Simplified geologic map of Fuji Volcano. There is no mappable unit for the Subashiri-a stage (8 to 5.6 ka), because this was a quiescent period without lava flows. Modified from Takada et al. (2016). Red triangles in the index map are Quaternary volcanoes; ER = Eurasia plate, PC = Pacific plate, PS = Philippine Sea plate

and compositional data of eruptive products from our new results (Takada et al. 2016; Yamamoto et al. 2020; Ishizuka et al. 2021), we report detailed variations of the eruption rate and the geochemistry of eruptive products since 5.6 ka, i.e., after a marked quiescence. Although the general framework for the changes in eruption rate including that period was reported by Miyaji (2007) and the chemical compositions of ejecta were described by Takahashi et al. (1991) and Kaneko et al. (2014), we here provide more detailed time-series data according to the new eruption stratigraphy (Additional file 1: Tables S1 and S2). As a result, our precise data show a more quantitative eruption history and give new insights into the relationship between the diversity of eruptive styles and magma compositions at Fuji Volcano.

Eruptive history of Fuji Volcano

Fuji Volcano has erupted basaltic magmas since its birth about 100 ka. However, the chemical compositions of eruptive products and the eruptive styles have not remained constant. For example, after 17 ka, incompatible element concentrations in the eruptive products changed (notably, the mean Zr/Y ratio increased from 2.8 to 3.3; e.g., Togashi and Takahashi 2007) and the eruptive style changed from explosive eruptions (the Hoshiyama stage) to effusion of voluminous lava flows (the Fujinomiya stage). The eruption activity decreased drastically during 8.0–5.6 ka, followed by a resumption of activity and rapid growth of a new edifice with the present summit crater (Miyaji 2007). Since 8 ka, the eruptive activity is defined as the Subashiri stage (Fig. 1), which has been divided into four substages (from -a to -d) based on the geological characteristics of the products by Takada et al. (2016) and summarized here. All eruptive products younger than 5.6 ka are listed in (Additional file 1: Table S1). The changes in the ratio of pyroclastic volume to total ejected volume shown in this study are consistent with the division of the substages (Fig. 2).

Subashiri-a stage (8.0–5.6 ka)

This substage was a period of relative quiescence during which only small volumes of basaltic scoria fall deposits were sparsely erupted without accompanying lava flows (S-0 to S-4 scoria eruptions; Miyaji 1988). The Fuji Black Soil formed around the volcano during this stage, creating a boundary between older (> 8.0 ka) and younger (Subashiri stage) tephra (Machida 1964).

Subashiri-b stage (5.6–3.45 ka)

Eruptive activity increased after the S-5 scoria eruption at 5.6 ka, resulting in the construction of the new volcanic edifice (Sb-ud in Table A1; total volume ca. 5 km^3 dense-rock equivalent, DRE), which comprises many thin basaltic lava flows emitted from the central conduit. Construction of the present summit region continued until 4.1 ka. Flank lava effusions occurred radially in all directions during this period, the largest being the Nihon-land lava flow (0.29 km^3 DRE) on the southern flank at 3.8 ka. Pyroclastic materials accounted for < 10% of the total mass of eruptive products during this substage (Fig. 2).

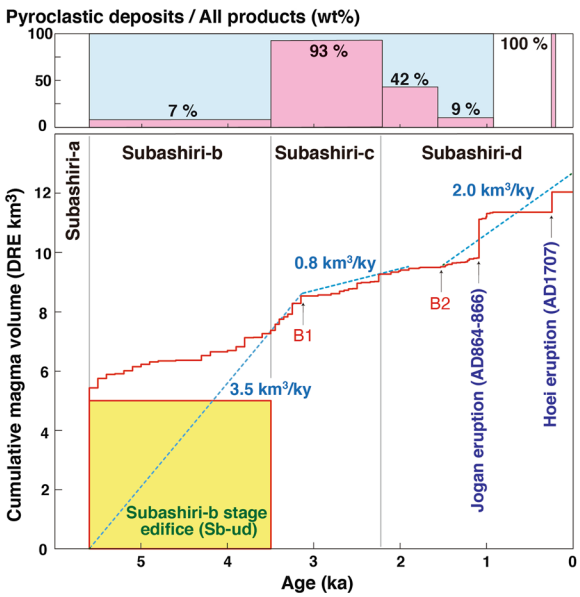

Fig. 2 Cumulated eruptive magma volumes and ratio of pyroclastic to all eruptive products. Because the volume of the Subashiri-b stage edifice cannot be subdivided for each eruption, the total volume is shown spanning the entire Subashiri-b stage. The eruptive volume and age of each eruption event is listed in (Additional file 1: Table S1). Blue dashed lines indicate the average eruption rate. B1 and B2 are bending points of the rate

Subashiri-c stage (3.45–2.25 ka)

Explosive basaltic sub-Plinian eruptions (S-10, Osawa, S-11, and S-12) occurred at the summit at the beginning of this substage, followed by explosive flank eruptions (Omuroyama-Katabutayama and S-13) that formed large scoria cones on the northwestern and southeastern flanks from 3.25 to 3.15 ka. Some pyroclastic fall deposits emplaced on the steep (> 34°) western flank repeatedly generated secondary basaltic pyroclastic flows (Yamamoto et al. 2005). The eastern flank of the edifice collapsed at 2.90 ka, producing the Gotenba debris avalanche. After the collapse, explosive basaltic eruptions from the summit became dominant. Conversely, explosive summit eruptions (Ginmeisui, Mishimadake, and Kengamine) from 2.60 to 2.25 ka deposited continuous agglutinate sheets on the upper flank, producing secondary rootless lava flows; the largest example was the Omuroyama-Katabutayama eruption, with a volume of

0.35 km^3 DRE. Pyroclastic materials accounted for > 90% of the total mass of eruptive products during this substage (Fig. 2).

Subashiri-d stage (2.25 ka to present)

The Kengamine eruption was the last summit eruption; subsequent recent eruptions were exclusively basaltic flank eruptions restricted to within 13.5 km of the summit. The frequency of flank eruptions increased to 20–30-year intervals during 1.5 to 1.0 ka, during which time pyroclastic materials accounted for < 10% of the total mass of eruptive products (Fig. 2). The AD 864–866 Jogan eruption, the largest since 5.6 ka, occurred on the lower northwestern flank and produced the Aokigahara lava flow (1.3 km^3 DRE; Chiba et al. 2007). Volcanic activity decreased from 0.9 to 0.3 ka. The Plinian AD 1707 Hoei eruption was the most recent eruption at Fuji, occurring on the southeastern flank 49 days after an M 8–9 earthquake along the Nankai trough. The volume erupted during this event was estimated at 0.68 km^3 DRE (Miyaji et al. 2011), and ash reached distal areas such as Tokyo. The first material erupted was dacite pumice, followed sequentially by andesitic and then basaltic scoria; eruptive products were exclusively pyroclastic materials (Fig. 2).

Eruption rates since 5.6 ka

The DRE eruptive volumes of each eruption, since 5.6 ka (Additional file 1: Table S1) were compiled by Ishizuka et al. (2021). Using this data set, we constructed a time variation diagram of the cumulative eruption volume at Fuji Volcano (Fig. 2). We did not subdivide the volumes of the many lava flows composing the Subashiri-b stage edifice (Sb-ud), but instead report their total volume for the overall duration of the edifice-building activities. The average eruption rate during the cone-building Subashiri-b stage was 3.5 km^3 DRE/kyr. Despite the change to explosive eruptions during the Subashiri-c stage, this high eruptive rate continued until 3.1 ka (B1 in Fig. 3). The eruption rate then markedly decreased to 0.8 km^3 DRE/kyr, although the relatively large sub-Plinian Mishimadake and Kengamine eruptions that ejected ~ 0.2 km^3 DRE each at 2.50 and 2.25 ka, respectively. Eruptive activity increased to an average eruptive rate of 2.0 km^3 DRE/kyr during the Subashiri-d stage, and more specifically from 1.5 ka (B2 in Fig. 3) until the Hoei eruption. However, eruption sizes and repose intervals were uneven during that period, and it is difficult to set a constant eruption rate as in the Subashiri-b and -c stages. For example, the Jogan eruption was much larger than other eruptions of this stage, and the average eruption rate varies greatly depending on the period selected. Furthermore, the abrupt Hoei eruption was preceded and followed by about 200 and 300 years of quiescence, respectively. The Hoei eruptive volume was also several times larger than those of sub-Plinian eruptions in the Subashiri-b and -c stages. Eruptive patterns, since 1.5 ka are thus quite different from those prior.

Petrological characteristics of the Subashiri-stage products

Various types of basaltic products have been erupted, since activity began at Fuji Volcano; these range from aphyric basalts to porphyritic ones with phenocryst assemblages comprising various combinations of plagioclase, olivine, clinopyroxene, and orthopyroxene. Basaltic andesite was occasionally erupted during the Subashiri-stage, and aphyric andesite–dacite magmas were ejected in association with basaltic products of the S-13 (3.15 ka) and AD 1707 Hoei eruptions. Although such SiO_2-rich magmas are rarely erupted, melt inclusions in olivine suggest that these intermediate to felsic magmas were preserved in shallow chambers as relicts of previous basaltic eruptions (Kaneko et al. 2010). Eruptive products at Fuji are thus dominated by hybrid magmas, but their mixing characteristics are not obvious from the whole-rock chemical compositions, because the contribution of basaltic magma tends to be very large.

Whole-rock compositions of all eruptive products, since 5.6 ka (Additional file 1: Table S2) contain 48.9–64.1 wt.% SiO_2, 15.8–19.5 wt.% Al_2O_3, 5.9–14.6 wt.% Fe_2O_3, 1.9–7.0 wt.% MgO, 5.2–10.8 wt.% CaO, 2.2–3.7 wt.% Na_2O, 0.4–2.1 wt.% K_2O, 0.9–2.0 wt.% Ti_2O, 6–43 ppm Rb, 316–496 ppm Sr, 15–39 ppm Y, and 41–159 ppm Zr. With increasing SiO_2 content, the products form a widely dispersed trend of increasing K_2O and Na_2O concentrations, constant Al_2O_3, TiO_2, Sr, and Y concentrations, and decreasing Fe_2O_3, MgO, and CaO concentrations (Additional file 2: Fig. S1). FeO*/MgO ratios range from 1.5 to 2.9 regardless of SiO_2 content, indicating that the basaltic magmas erupted throughout this stage were highly differentiated. These results are consistent with previous studies (Togashi et al. 1991; Takahashi et al. 1991; 2003; Kaneko et al. 2014).

Temporal variations in geochemical compositions since 5.6 ka

Although eruption styles varied among the Subashiri substages, the chemical compositions of the eruption products do not show corresponding changes, except for some elements. Excluding the andesite–dacite magmas produced during the S-13 and Hoei eruptions, SiO_2 contents ranged from 48.9 to 53.5 wt.%, almost unchanged throughout the entire stage (Fig. 3). MgO contents during the Subashiri-b stage (4.5–7.0 wt.%) were higher than those during the Subashiri-c (4.2–6.2 wt.%) and -d stages (4.3–6.3 wt.%, excluding andesite–dacite); MgO

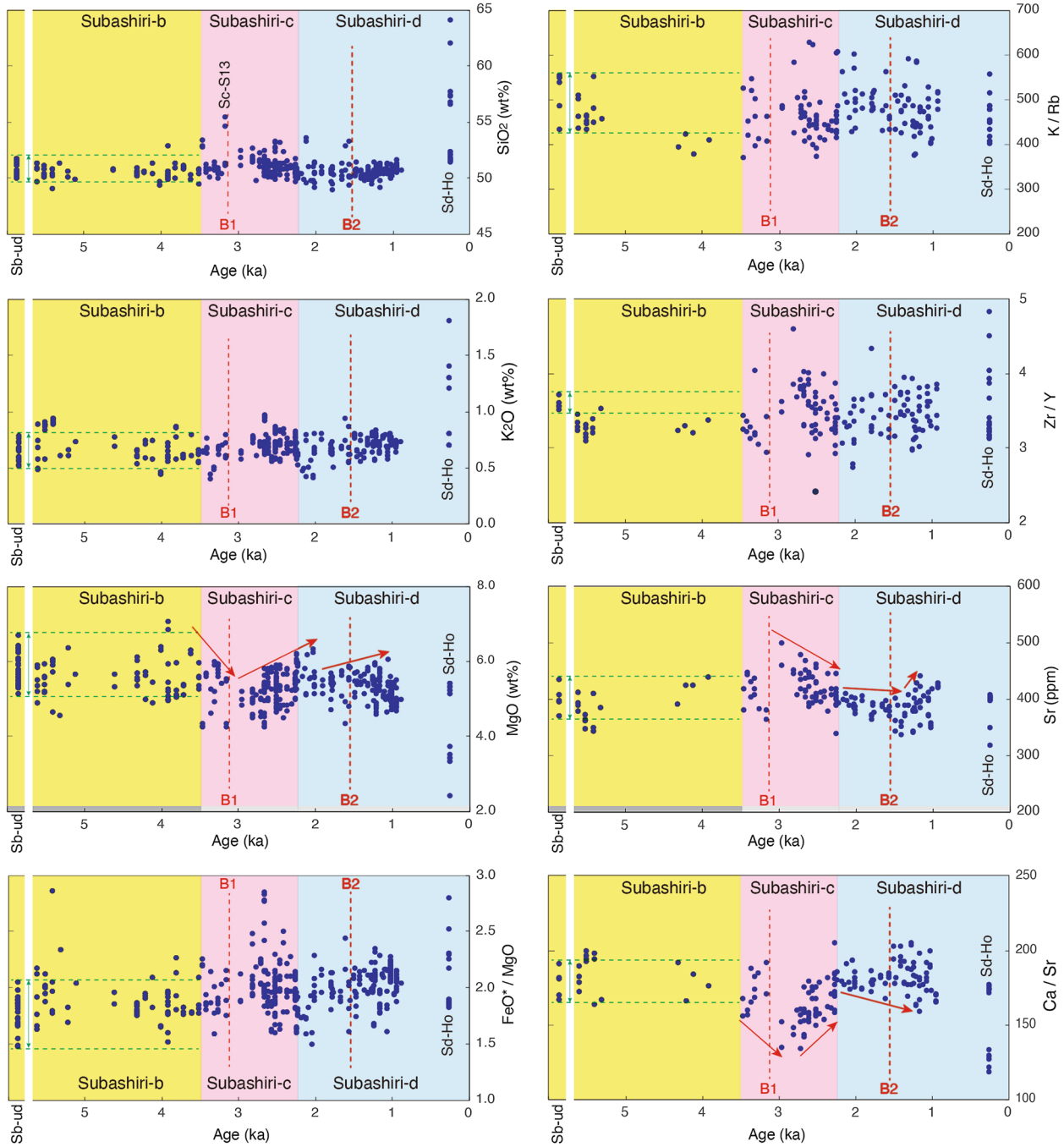

Fig. 3 Temporal variations of the geochemistry of eruptive products since 5.6 ka. Green dashed lines indicate the geochemical range of the Subashiri-b stage edifice (Sb-ud). B1 and B2 are bending ages of the eruption rate in Fig. 2. Sc-S13 = the S-13 eruption (3.15 ka), Sd = Ho = AD 1707 Hoei eruption

contents have a large variance and these ranges largely overlap. At around B1, when the eruption rate started to decline, MgO content decreased, but then recovered to the original level (Fig. 3). Although large dispersions of K_2O content and FeO*/MgO ratio are characteristic of Fuji eruptive products, their compositional ranges have hardly changed throughout the stage (Fig. 3). Al_2O_3, Fe_2O_3, CaO, Na_2O and TiO_2 contents are also the same throughout the Subashiri stage (Additional file 2: Fig. S1). The ratios of incompatible elements in basaltic magmas,

such as K/Rb and Zr/Y, did not notably change during the Subashiri stage (Fig. 3) as they had, for example, around 17 ka. Furthermore, except for the Hoei eruption, rare earth element (REE) abundances were similar during the three substages (Additional file 2: Fig. S2).

One compositional feature that has changed during the Subashiri substages is Sr content (Fig. 3); Sr contents during the Subashiri-c stage were 337–496 ppm, a range marked by a slightly higher upper limit than those during the Subashiri-b (341–438 ppm) and -d stages (334–439 ppm). This difference is more pronounced looking at the Ca/Sr ratio (Fig. 3); the range of Ca/Sr during the Subashiri-c stage (133–204) has a distinctly lower limit than those during the Subashiri-b (162–197) and -d stages (158–202, excluding andesite–dacite). The Sr content and Ca/Sr ratio were maximum and minimum immediately after B1, and then gradually decreased and increased during the Subashiri-c stage, respectively.

Discussion

Following the period of quiescence from 8 to 5.6 ka, activity during the Subashiri-b stage resumed, erupting basaltic magmas at a rate of 3.5 km^3 DRE/kyr (Fig. 2). This long-term eruption rate is among the highest of active volcanoes in Japan (Yamamoto et al. 2018) but an order of magnitude lower than the average for active basaltic volcanoes worldwide (White et al. 2006). The lack of eruption of SiO_2-rich magma at the time of the resumption suggests that the contribution of differentiated magma, which may be residue of preceding activity and evolved by fractional crystallization during the quiescence, was small. In other words, the massive injection of new basaltic magma led to the resumed activity at 5.6 ka. This magma plumbing system was stable until 3.45 ka, when the eruption style shifted from effusive to explosive. In particular, the changes in MgO content and Ca/Sr ratio from the Subashiri-b to -c stages (Fig. 3), while the amounts of other elements remained constant, suggest that some difference occurred in the magma differentiation system.

On the basis of petrological observations, Kaneko et al. (2010) proposed that Fuji's plumbing system comprises at least two magma chambers: a deeper (~20 km depth) basaltic one and a shallower (~8–9 km depth) more SiO_2-rich one. Indeed, a zone of low seismic velocity at ~20 km depth has been attributed to the presence of a magma chamber (Lees and Ukawa 1992; Ukawa 2005; Nakamichi et al. 2007). This lower chamber is deeper than those of other volcanoes along the Izu-Mariana arc (such as Izu-Oshima volcano, whose magma reservoir is at < 10 km depth; Mikada et al. 1997; Kaneko et al. 2019), and its depth corresponds to the bottom of the granitic middle crust of the Philippine Sea plate beneath the Eurasian plate (Fujii 2007). Within the lower chamber, the prevalent fractional crystallization of pyroxenes together with calcic plagioclase and olivine (an assemblage with SiO_2 content similar to that of the liquid) under high pressure results in an increase in K_2O content and FeO*/MgO, while the SiO_2 content remains in the basaltic range (Fujii 2007). Furthermore, the observed increase in Al_2O_3 content relative to MgO (Fig. 4) has been attributed to the delayed fractionation of plagioclase relative

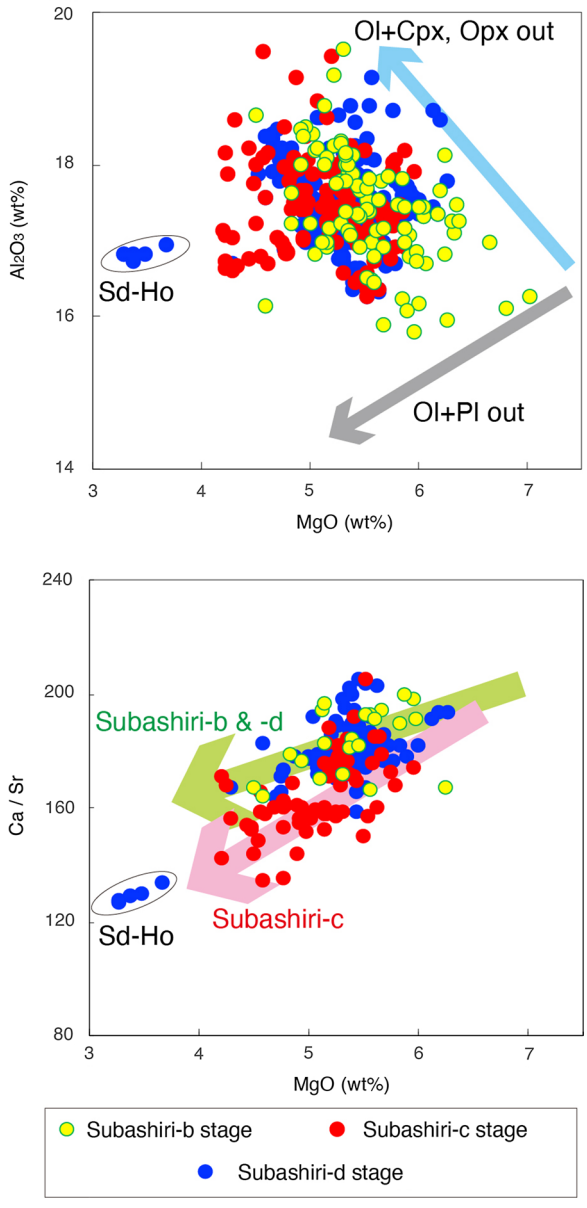

Fig. 4 Al_2O_3–MgO and Ca/Sr-MgO variation diagrams of the Subashiri stage products (Ol, olivine; Cpx, clinopyroxene; Opx, orthopyroxene; Pl, plagioclase)

to pyroxenes in the lower chamber at high pressure (Hamada and Fujii 2007).

The transition from the Subashiri-b to -c stages is marked by a transition from effusive to explosive eruptions. However, the similarity of the K/Rb and Z/Y ratios (Fig. 3) and REE patterns (Additional file 2: Fig. S2) of eruptive products during both stages indicates that the geochemistry of the parental magma was similar. The main geochemical differences between the substages are Sr content and Ca/Sr ratio (Fig. 3), which are indicative of plagioclase fractionation. Because Sr replaces Ca in plagioclase, this change in Ca/Sr ratio indicates that plagioclase played a different role during crystal fractionation. The decrease in Ca/Sr relative to MgO was greater during the Subashiri-c stage than during the -b and -d stages (Fig. 4), indicating reduced plagioclase fractionation during the Subashiri-c stage. Indeed, high-pressure experiments on hydrous basalts show that plagioclase experiences the greatest decrease in crystallization temperature under increasingly hydrous conditions (Baker and Eggler 1983; Sisson and Grove 1993). There is no significant gap in FeO*/MgO ratio between those large and small Ca/Sr magmas; it is unlikely that there was a large difference in the degree of differentiation between them, increasing the water content. Therefore, the decreased Ca/Sr ratios of Subashiri-c stage products indicates that the water content of the injected parental magma was greater than during the other substages, consistent with the predominance of explosive eruptions during the Subashiri-c stage. Although controls on explosive–effusive eruption styles depends on a set of feedback involving magma viscosity, ascending speed and gas loss (e.g., Cassidy et al. 2018), the most important factor is the water content of the primary magma.

After the last explosive summit eruption (Kemgamine) at 2.25 ka, flank fissure eruptions have prevailed during the Subashiri-d stage. In response to this change, Ca/Sr ratios of the Subashiri-c stage products increased to the level of the Subashiri-b stage, when lava-flow extrusion was dominant (Fig. 3). Similar magmas in term of compositions, fed both the central conduit system during the Subashiri-b stage and flank fissure vents during the most recent activities. Takada (1997) and Takada et al. (2007) attributed variations in the plumbing system between a central conduit and flank fissures to stress accumulation due to magma intrusions being accommodated by stress relaxation, although they did not clarify any specific subsurface changes. After the Kengamine eruption, eruptive volumes were clearly reduced for ~ 1 kyr. At 1.5 ka (B2 in Fig. 2), the frequency of eruptions began to increase, and the largest eruption in the Subashiri stage, the Jogan eruption, occurred during this flare-up. On the other hand, the chemical composition of the erupted materials did not change significantly before and after B2 (Fig. 3). The site, size, and repose intervals of eruptions have become more variable since 1.5 ka; the regularity of eruptions during the Subashiri-b and -c stages is no longer observed. This detailed eruptive history makes it difficult to predict the next eruptive pattern at Fuji Volcano, and various possibilities in eruption styles must be considered. Thus, the revised March 2021 hazard map reasonably includes predictions of disaster areas for recurrences of all past eruption events.

Conclusions

Based on a new stratigraphic sequence by Takada et al. (2016), we used time-series data on eruptive volumes and the geochemistry of eruptive products to clarify temporal variations of eruption rate and magma composition during the Subashiri stage of Fuji Volcano (i.e., since the quiescent period during 8.0–5.6 ka). This stage comprises the formation of a new volcanic edifice composed of many thin lava flows during 5.6–3.45 ka, explosive eruptions at the summit and on the flanks of the volcano during 3.45–2.25 ka, and a transition to dominantly flank fissure eruptions since 2.25 ka. The eruption rate decreased from 3.5 km^3 DRE/kyr during the edifice-building period to 0.8 km^3 DRE/kyr during the explosive eruption period and then increased to 2.0 km^3 DRE/kyr after 1.5 ka. Although repeated, similar eruptions occurred during the edifice-building and explosive eruption periods, the sites, sizes, and repose intervals of eruptions, since 1.5 ka have not been regular. Magmas erupted during the Subashiri stage are dominantly basaltic in composition and largely geochemically similar, except for increased Sr contents and decreased Ca/Sr ratios during the explosive eruption period. This finding indicates that although the geochemical properties of the parental magmas were nearly constant throughout the stage, an increase in the water contents of the parental magmas during the explosive eruption period resulted in the delayed fractionation of plagioclase. The results of this study show that the changes in eruption patterns and eruption rates are linked to geochemical changes, which will be an important guideline for predicting future volcanic activity.

Supplementary Information

The online version contains supplementary material available at https://doi.org/10.1186/s40623-021-01505-1.

Additional file 1: Table S1. List for the eruption products of Fuji Volcano during the Subashiri stage. **Table S2.** Compilation of major and trace element composition for the products of Fuji Volcano during the Subashiri stage.

Additional file 2: Figure S1. Harker variation diagrams for the Subashiri-stage products of Fuji Volcano. **Figure S2.** Chondrite-normalized REE patterns for the Subashiri-stage products of Fuji Volcano.

Acknowledgements
This study is an outgrowth of the geologic mapping project of the Geological Survey of Japan, AIST. We thank Akira Takada for his collaborative efforts in our field research. Discussions in the Review Committee of Volcanic Hazard Map of Fuji Volcano (Chair: Toshitsugu Fujii) were beneficial to this study. Instructive discussions and detailed comments by the reviewers significantly improve this paper.

Authors' contributions
TY, SN and YI: all of the authors participated in field research, analyzed the samples, measured the amount of eruption, and discussed the results. All authors read and approved the final manuscript.

Funding
We have no funding for the research reported should be declared.

Availability of data and materials
The age and volume for the eruptions and the geochemical data of the samples are listed in Additional file 1: Tables S1 and S2, respectively.

Declarations

Ethics approval and consent to participate
Not applicable.

Consent for publication
Not applicable.

Competing interests
The authors declare that they have no competing financial interests.

Received: 9 June 2021 Accepted: 17 August 2021
Published online: 27 August 2021

References

Baker DR, Eggler DH (1983) Fractionation paths of Atka (Aleutians) high-alumina basalts: constraints from phase relations. J Volcanol Geotherm Res 18:387–404

Cassidy M, Manga M, Cashman K, Bachmann O (2018) Controls on explosive-effusive volcanic eruption styles. Nat Commun 9:2839. https://doi.org/10.1038/s41467-018-05293-3

Chiba T, Tomita Y, Suzuki Y, Arai K, Fujii N, Miyaji N, Koizumi S, Nakashima K (2007) Analysis of micro topography of the Aokigahara lava flows, Fuji volcano, by the light detection and ranging system. In: Aramaki S, Fujii T, Nakada S, Miyaji N (eds) Fuji Volcano. Yamanashi Inst Environ Sci, Fuji-Yoshida, pp 349–363 (**in Japanese with English abstract**)

Fujii T (2007) Magmatology of Fuji Volcano. In: Aramaki S, Fujii T, Nakada S, Miyaji N (eds) Fuji Volcano. Yamanashi Inst Environ Sci, Fuji-Yoshida, pp 233–244 (**in Japanese with English abstract**)

Hamada M, Fujii T (2007) Experimental constraints on the effects of pressure and H_2O on the fractional crystallization of high-Mg island arc basalt. Contrib Mineral Petrol 155:767–790. https://doi.org/10.1007/s00410-007-0269-6

Ishizuka Y, Yamamoto T, Nakano S, Yoshimoto M (2021) Estimated eruption volume of the Subashiri-stage products during the last 7,000 years, Fuji Volcano, Japan. Open-File Rep Geol Surv Japan AIST, no.715 (**in Japanese with English abstract**)

Kaneko K, Mishiro K, Tatsumi Y (2019) Control of volcanic activity by crustal structure: inference from the Izu-Bonin-Mariana and Northeast Japan arcs. Geophy Res Lett 46:12968–12976. https://doi.org/10.1029/2019gl084554

Kaneko T, Yasuda A, Fujii T, Yoshimoto M (2010) Crypto-magma chambers beneath Mt. Fuji J Volcanol Geotherm Res 193:161–170. https://doi.org/10.1016/j.jvolgeores.2010.04.002

Kaneko T, Yasuda A, Shimano T, Yoshimoto M, Fijii T (2014) Whole-rock chemical composition of scoria layers of the younger stage exposing at Taro-bo, Mt Fuji: a change in the magma plumbing system occurred around formation period of the Fuji-black soil layer (FB). Bull Volcanol Soc Japan 59:41–54 (**in Japanese with English abstract**)

Lees JM, Ukawa M (1992) The South Fossa Magna, Japan, revealed by high-resolution P- and S-wave travel time tomography. Tectonophysics 208:377–396. https://doi.org/10.1016/0040-1951(92)90436-A

Machida H (1964) Tephrochronological study of Volcano Fuji and adjacent areas. J Tokyo Geogr Soc 73(293–308):337–350 (**in Japanese with English abstract**)

Mikada H, Watanabe H, Sakashita S (1997) Evidence for subsurface magma bodies beneath Izu-Oshima volcano inferred from a seismic scattering analysis and possible interpretation of the magma plumbing system of the 1986 eruptive activity. Phys Earth Planet Inter 104:257–269. https://doi.org/10.1016/S0031-9201(97)00060-5

Miyaji N (1988) History of younger Fuji Volcano. J Geol Soc Japan 94:433–452 (**in Japanese with English abstract**)

Miyaji N (2007) Eruptive history, eruption rate and scale of eruptions for the Fuji Volcano during the last 11,000 years. In: Aramaki S, Fujii T, Nakada S, Miyaji N (eds) Fuji Volcano. Yamanashi Inst Environ Sci, Fuji-Yoshida, pp 79–95 (**in Japanese with English abstract**)

Miyaji N, Kan'no A, Kanamaru T, Mannen K (2011) High-resolution reconstruction of the Hoei eruption (AD 1707) of Fuji volcano, Japan. J Volcanol Geotherm Res 207:13–129. https://doi.org/10.1016/j.jvolgeores.2011.06.013

Nakamichi H, Watanabe H, Ohminato T (2007) Three-dimensional velocity structures of Mount Fuji and the South Fossa Magna, central Japan. J Geophy Res 112:B03310. https://doi.org/10.1029/2005jb004161

Sisson TW, Grove TL (1993) Experimental investigations of the role of H_2O in calc-alkaline differentiation and subduction zone magmatism. Contrib Mineral Petrol 113:143–166. https://doi.org/10.1007/bf00283225

Takada A (1997) Cyclic flank-vent and central-vent eruption patterns. Bull Volcanol 58:539–556

Takada A, Yamamoto T, Ishizuka Y, Nakano S (2016) Geologic map of Fuji Volcano. Second edition. Geol Surv Japan AIST, Tsukuba

Takada A, Ishizuka Y, Nakano S, Yamamoto T, Kobayashi M, Suzuki, Y (2007) Characteristic and evolution inferred from eruptive fissures of Fuji volcano, Japan. In: Aramaki S, Fujii T, Nakada S, Miyaji N (eds) Fuji Volcano. Yamanashi Inst Environ Sci, Fuji-Yoshida, pp 183–202 (**in Japanese with English abstract**)

Takahashi M, Hasegawa Y, Tsukui M, Nemoto Y (1991) Evolution of magma-plumbing system beneath Fuji Volcano: on the view point of whole-rock chemistry. Bull Volcanol Soc Japan 36:281–296 (**in Japanese with English abstract**)

Takahashi M, Kominami M, Nemoto Y, Hasegawa Y, Nagai T, Tanaka H, Nishi N, Yasui M (2003) Whole-rock chemistry for eruptive products of Fuji Volcano, Central Japan: summary of analytical data of 847 samples. Proc Inst Nat Sci Nihon Univ 38:117–166 (**in Japanese with English abstract**)

Togashi S, Takahashi M (2007) Geochemistry of rocks from the Fuji volcano, Japan; constraints for evolution of magmas. In: Aramaki S, Fujii T, Nakada S, Miyaji N (eds) Fuji Volcano. Yamanashi Inst Environ Sci, Fuji-Yoshida, pp 219–231 (**in Japanese with English abstract**)

Togashi S, Miyaji N, Yamazaki H (1991) Fractional crystallization in a large tholeiitic magma chamber during the early stage of the Younger Fuji Volcano, Japan. Bull Volcanol Soc Japan 36:269–280 (**in Japanese with English abstract**)

Ukawa M (2005) Deep low-frequency earthquake swarm in the mid crust beneath Mount Fuji (Japan) in 2000 and 2001. Bull Volcanol 68:47–56. https://doi.org/10.1007/s00445-005-0419-5

White SM, Crisp JA, Spera FJ (2006) Long-term volumetric eruption rates and magma budgets. Geochem Geophy Geosys 7:3. https://doi.org/10.1029/2005gc001002

Yamamoto T, Nakada S. (2015) Extreme Volcanic Risks 2: Mount Fuji. In: Shroder JF, Papale P (eds) Volcanic Hazards, Risks, and Disasters. Elsevier, Amsterdam, pp 355–376. https://doi.org/10.1016/B978-0-12-396453-3.00014-9

Yamamoto T, Kudo T, Isizuka O (2018) Temporal variations in volumetric magma eruption rates of Quaternary volcanoes in Japan. Earth Planets Space 70:65. https://doi.org/10.1186/s40623-018-0849-x
Yamamoto T, Nakano S, Ishizuka Y, Takada A (2020) Quantitative re-description of the younger pyroclastic fall deposits ejected from Fuji Volcano, Japan. Bull Geol Surv Japan 71:517–580 (**in Japanese with English abstract**)
Yamamoto T, Takada A, Ishizuka Y, Miyaji N, Tajima Y (2005) Basaltic pyroclastic flows of Fuji volcano, Japan: characteristics of the deposits and their origin. Bull Volcanol 67:622–633. https://doi.org/10.1007/s00445-004-0398-y

Publisher's Note